Nanoscale

PAPER

View Article Online
View Journal | View Issue

Cite this: *Nanoscale*, 2015, **7**, 171

Interactions between lipid-free apolipoprotein-AI and a lipopeptide incorporating the RGDS cell adhesion motif

V. Castelletto,*†[a] I. W. Hamley,[a] M. Reza[b] and J. Ruokolainen[b]

Received 1st September 2014,
Accepted 19th October 2014

DOI: 10.1039/c4nr05072j

www.rsc.org/nanoscale

The interaction of a designed bioactive lipopeptide C_{16}-GGGRGDS, comprising a hexadecyl lipid chain attached to a functional heptapeptide, with the lipid-free apoliprotein, Apo-AI, is examined. This apolipoprotein is a major component of high density lipoprotein and it is involved in lipid metabolism and may serve as a biomarker for cardiovascular disease and Alzheimers' disease. We find *via* isothermal titration calorimetry that binding between the lipopeptide and Apo-AI occurs up to a saturation condition, just above equimolar for a 10.7 μM concentration of Apo-AI. A similar value is obtained from circular dichroism spectroscopy, which probes the reduction in α-helical secondary structure of Apo-AI upon addition of C_{16}-GGGRGDS. Electron microscopy images show a persistence of fibrillar structures due to self-assembly of C_{16}-GGGRGDS in mixtures with Apo-AI above the saturation binding condition. A small fraction of spheroidal or possibly "nanodisc" structures was observed. Small-angle X-ray scattering (SAXS) data for Apo-AI can be fitted using a published crystal structure of the Apo-AI dimer. The SAXS data for the lipopeptide/Apo-AI mixtures above the saturation binding conditions can be fitted to the contribution from fibrillar structures coexisting with flat discs corresponding to Apo-AI/lipopeptide aggregates.

Introduction

Apolipoproteins are proteins that bind lipids, and are involved in lipid transport *in vivo*. There are six classes of apolipoprotein with different structures and biological activities. The apoliprotein A family is a major component of high density lipoprotein (HDL). HDL removes fat and cholesterol from cells and therefore there is significant research interest in the interaction of Apo-A apolipoproteins with lipids due to biomedical relevance, in particular to cardiovascular disease. Among this class, Apo-AI is the major component of HDL, comprising 70% of total protein.[1] Polymorphism in the gene associated with Apo-AI has been associated with early onset Alzheimer's disease.[2]

The structure of Apo-AI comprises two domains – the N terminal (residue 1–186) domain comprises a four-helix bundle of amphipathic α-helices that result from 11- and 12-residue repeats, whilst the C terminal domain comprises two further helices, when bound to lipid although less ordered in the absence of lipid.[3–5] Apolipoproteins such as Apo-AI may adopt a necklace-like structure[6] (Fig. 1) and these are able to wrap around bundles of lipid molecules to form so-called "nanodiscs".[7,8]

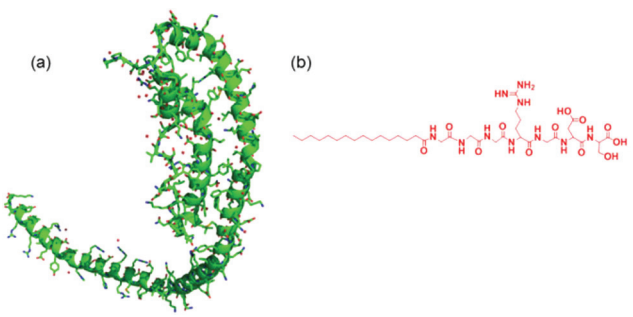

Fig. 1 Structure of (a) Apo-AI (pdb file 3R2P,[23]), (b) Lipopeptide C_{16}-GGGRGDS.

The interaction of Apo-AI with various lipids has been the subject of several studies which indicate that binding between the apolipoprotein and lipids leads to enhanced α-helix content.[9–11] The binding is believed to be achieved *via* the C-terminal α-helices in Apo-AI[5,10] which insert into lipid membranes. There is a concomitant increase in α-helical content in the C terminal domain along with a second step conformational transition in the N terminal helix bundle exposing the helices to lipid.[12] Binding leads to the formation of HDL-like

[a]*Department of Chemistry, University of Reading, Whiteknights, Reading, RG6 6AD, UK. E-mail: I.W.Hamley@reading.ac.uk*
[b]*Department of Applied Physics, Aalto University School of Science, P.O. Box 15100 FI-00076 Aalto, Finland*
†Current address: National Physical Laboratory, Hampton Rd, Teddington, Middlesex TW11 0LW, UK.

aggregates including nascent discoidal particles and circulating spherical particles.[12–14]

Here, we investigate for the first time to our knowledge, the interaction of Apo-AI with a designed lipopeptide. We selected the lipopeptide C_{16}-GGGRGDS (G: Glycine, R: Arginine, D: Aspartic Acid and S: Serine) because firstly it contains a bioactive cell adhesion motif (RGDS) which has been exploited by us in applications in cell culture supports for tissue engineering.[15,16] Similar lipopeptides have been used by others in materials for tissue engineering and other cell-based therapeutic materials.[17,18] Second, its self-assembly has been extensively characterized by ourselves[19] and that of similar peptide amphiphiles has been extensively examined by others.[20]

Experimental

Materials

Apolipoprotein A-I (Apo-AI), a high density lipoprotein extracted from human plasma, was purchased from Calbiochem (US) and received as a stock solution containing 53.6 μM Apo-AI in 10 mM NH_4HCO_3 (pH 7.4). The Apo-I molecular weight (M_w) is 28 kDa. Lipopeptide C_{16}-GGGRGDS was custom synthesized by CS Bio (Menlo Park, USA) as a TFA salt. The purity was 95.46% (by analytical HPLC in a TFA water/acetonitrile gradient). M_W was obtained by electrospray-mass spectrometry. $M_{w,Found}$ = 842.99 and $M_{w,Expected}$ = 842.40.

Sample preparation

53.6 μM Apo-AI stock solution was diluted in 10 mM Tris, 0.1 mM NaCl (pH 7.4), while aqueous C_{16}-GGGRGDS solutions were prepared at pH 8, by titrating 0.1 M NaOH. Binary samples were made by mixing weighed solutions of Apo-AI and C_{16}-GGGRGDS at different molar ratios M_r = [C_{16}-GGGRGDS]/[Apo-AI].

Circular dichroism (CD)

Spectra were recorded using a Chirascan spectropolarimeter (Applied Photophysics, UK). The sample was placed in a cover slip cuvette (0.01 cm thick). Spectra are presented with absorbance $A < 2$ at any measured point with a 0.5 nm step, 1 nm bandwidth, and 1 second collection time per step at 20 °C. The post-acquisition smoothing tool from Chirascan software was used to remove random noise elements from the averaged spectra. A residual plot was generated for each curve in order to verify whether or not the spectrum had been distorted during the smoothing process. The CD signal from the water was subtracted from the CD data of the peptide solutions. The spectra were collected as ellipticity θ as a function of wavelength and converted to mean residue molar ellipticity $[\theta] = \theta/(l10c)$ using the sample molar concentration $c = 243 \times c_1 + 7 \times c_2$ (c_1: molar concentration of Apo-AI, 243: number of residues on Apo-AI, c_2: molar concentration of C_{16}-GGGRGDS, 7: number of residues on C_{16}-GGGRGDS).

Small-angle X-ray scattering (SAXS)

Experiments were performed on beamline BM29 at the ESRF (Grenoble, France). A few microlitres of samples were injected *via* an automated sample exchanger at a slow and very reproducible flux into a quartz capillary (1.8 mm internal diameter), which was then placed in front of the X-ray beam. The quartz capillary was enclosed in a vacuum chamber, in order to avoid parasitic scattering. After the sample was injected in the capillary and reached the X-ray beam, the flow was stopped during the SAXS data acquisition. The sample was thermostated throughout its entire travel from the injector to the quartz capillary. SAXS experiments were performed at 20 °C. The $q = 4\pi\sin\theta/\lambda$ range was set to 0.04–4 nm^{-1}, with λ = 0.1 nm (12 keV). The images were captured using a PILATUS 1M detector. Data processing (background subtraction, radial averaging) was performed using dedicated beamline software ISPYB.

SAXS theory

The SAXS data for the 10 μM Apo-AI (M_r = 0) was modelled using the software Crysol (Version 2.8 ©ATSAS team 1995–2011).[21,22] Crysol evaluates the solution scattering from macromolecules with known atomic structure. In this work, we used the atomic coordinates for the structure of C Terminal Truncated Human Apolipoprotein A-I listed in the Protein Databank File pdb file 3R2P.[23] The crystal structure is displayed in Fig. 1a. SAXS data for samples with M_r = 2.2–14.9 was modelled according to a co-existence of flat cylinders, with diameter D and length L, with bilayer tapes described as Gaussian bilayers interacting through the Caillé structure factor for multi-layer systems. The details of the model used to describe the bilayers are provided elsewhere.[19,24–26] The model assumes an electron density profile comprising one Gaussian function for each headgroup on either side of the bilayer electron density (ρ_H) profile, and one Gaussian function for the chains in the core of the bilayer electron density (ρ_C) profile. The position of the Gaussian peaks is at z_H and z_C for ρ_H and ρ_C respectively. The model assumes a standard deviation σ_H and σ_C for z_H and z_C respectively, while the bilayer is centred at $z = z_C = 0$. We used a Gaussian distribution of z_H, with associated degree of polydispersity Δ_{ZH}. The background was taken to be a constant C_0. The fitting parameters of the model are z_H, ρ_H, σ_H, ρ_C, σ_C and C_0. The modified Caillé theory appropriate for lamellar systems corresponds to a multilayer structure influenced by thermal fluctuations. It is described by the total number of layers N, the layer spacing d and the Caillé parameter η.[25,26]

Cryo-transmission electron microscopy (cryo-TEM)

Experiments were carried out using a field emission cryo-electron microscope (JEOL JEM-3200FSC) operating at 200 kV. Images were taken using bright-field mode and zero loss energy filtering (omega type) with a slit with 20 eV. Micrographs were recorded using a Gatan Ultrascan 4000 CCD camera. The specimen temperature was maintained at −187 °C during the imaging. Vitrified specimens were prepared using

an automated FEI Vitrobot device using Quantifoil 3.5/1 holey carbon copper grids with 3.5 μm hole sizes. Grids were cleaned using a Gatan Solarus 9500 plasma cleaner just prior to use and then transferred into an environmental chamber of an FEI Vitrobot at room temperature and 100% humidity. Thereafter, 3 μl of sample solution at 2 wt% concentration was applied on the grid, blotted once for 1 second and then vitrified in a 1/1 mixture of liquid ethane and propane at −180 °C. Grids with vitrified sample solutions were maintained in a liquid nitrogen atmosphere and then cryo-transferred into the microscope.

Transmission electron microscopy (TEM)

TEM imaging was performed using a Philips CM20 TEM microscope operated at 200 kV. Droplets of solutions were placed on Cu grids coated with a carbon film (Agar Scientific, UK), stained with 1 wt% uranyl acetate, and air-dried.

Isothermal titration calorimetry (ITC)

ITC experiments were carried out using an iTC200 microcalorimeter. The Apo-AI stock solution (53.6 μM Apo-AI diluted in 10 mM NH_4HCO_3, pH 7.4) was dissolved to give a 10.7 μM solution of Apo-AI using 10 mM Tris, 0.1 mM NaCl, pH 7.4. The working cell was filled with 200 μL of the 10.7 μM Apo-AI solution and the reference cell was filled with deionized water. The titrant syringe was filled with a solution of 1.54 mM C_{16}-GGGRGDS (dissolved in the same buffer used for the Apo-AI solution in the working cell). The ITC experiment was programmed to run 18 injections of 2 μL volume of the titrant solution (1.54 mM C_{16}-GGGRGDS) into the working cell (10.4 μM of Apo-AI) with 180 s lag between each injection to ensure return to the baseline. The syringe was stirred throughout the experiment at 750 rpm and the working cell was set at 25 °C. The data was analysed using Origin 7 (MicroCal) by fitting the curve using the one set of sites model.

Results

To first probe the possible interactions between Apo-AI and C_{16}-GGGRGDS (Fig. 1 shows, respectively the structure of Apo-AI from X-ray crystallography and a molecular model of the PA) we employed isothermal titration calorimetry (ITC), a well-known technique to enable investigation of the molecular interactions of biological samples, in this case a protein-lipopeptide interaction. The experiment was designed to inject 1.54 mM C_{16}-GGGRGDS into 53.6 μM Apo-AI, *i.e.* C_{16}-GGGRGDS is the ligand and Apo-AI is the receptor. The relatively low Apo-AI concentration selected for ITC reduces the total number of binding sites to ensure saturation of C_{16}-GGGRGDS binding to Apo-AI is reached. The ITC profile for the titration of C_{16}-GGGRGDS into Apo-AI (Fig. 2a) exhibits a series of positive peaks, indicating an endothermic reaction. The integration and normalization of the endothermic peaks produced a sigmoidal curve relative to the moles of ligand added, which was then appropriately fitted to a one set of sites

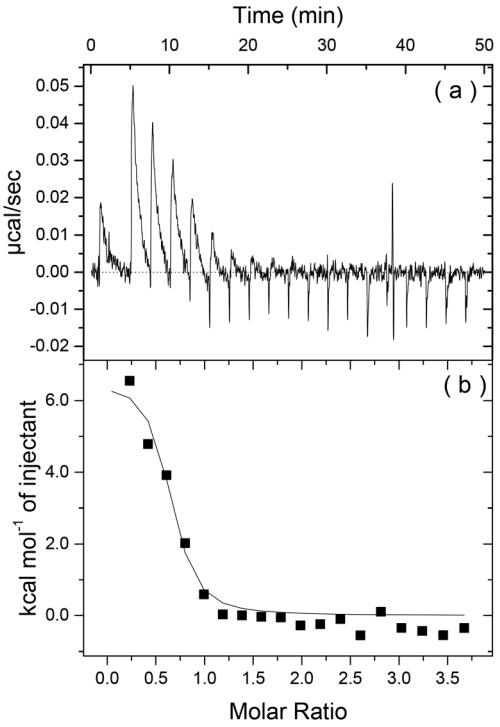

Fig. 2 (a) Heat release as a function of time and (b) energy released as a function of the molar ratio for Apo-I titrated with C_{16}-GGGRGDS.

model. The one set of sites model was used for the peptide/lipopeptide system as it is assumed that each binding site has the same binding affinity. A binding constant $K = (3.21 \pm 1.7) \times 10^6$ M^{-1} was determined from the fitting parameters (Fig. 2b). Other parameters including the number of binding sites $N = (0.59 \pm 0.04)$, enthalpy $\Delta H = (6.6 \pm 0.6)$ kcal mol^{-1} and entropy $\Delta S = 0.05$ Kcal mol^{-1} $°C^{-1}$ were also obtained from the fit.

Fig. 2b shows that the system reaches saturation at $M_r = 1.2$, because only heat of dilution is observed for $M_r > 1.2$. ΔH reflects the strength of the ligand/target interaction enthalpy relative to that with solvent, primarily due to hydrogen bond formation and van der Waals interactions. It is highly unlikely that an endothermic reaction ($\Delta H > 0$), is dominated by hydrogen bonding or van der Waals interactions. The isotherm corresponds to a favourable change in entropy ($-T\Delta S < 0$). Therefore it is possible that Apo-AI/C_{16}-GGGRGDS binding is driven by hydrophobic interactions. The ITC signal is a result of many interactions – not just the binding process of Apo-AI to the lipopeptide but also potential protein conformational changes upon dilution, lipopeptide/lipopeptide and hydration effects. However, an unfavourable ΔH associated with an endothermic process is possibly due to conformational constraints of the Apo-AI.[27]

To our knowledge, there are no prior reports on binding of Apo-AI to lipopeptides. ITC experiments have been mostly performed to study the binding of lipids to Apo-AI. Although these experiments show that lipids bind to Apo-AI at room temperature through an exothermic reaction,[10,28–30] one report shows an endothermic reaction for the titration of Apo-AI into

1-palmitoyl,2-oleoyl phosphatidylcholine/sphingomyelin small unilamellar vesicles at 37 °C.[29]

Having determined M_r = 1.2 as the saturation limit for Apo-AI/C_{16}-GGGRGDS binding at 10.7 μM protein (Fig. 2), further studies were performed for a fixed concentration of 10.7 μM Apo-AI, to allow for comparison with results from ITC experiments.

The influence of interactions between Apo-AI and the lipopeptide C_{16}-GGGRGDS on the secondary structure of the lipopeptide were examined by CD spectroscopy. CD spectra for mixtures with M_r = 2.2–14.4 are shown in Fig. 3a. Fig. 3b shows the dependence with M_r of the ellipticity at the minima at 209 and 221 nm. Again, saturation is observed above equimolar conditions. The results in Fig. 3 show that the amount of alpha-helix secondary structure decreases upon increasing M_r. Previous studies have shown that human Apo-AI has high α-helical content, values between 43%–68% having been reported,[1,9–11,31] in good agreement with the CD for pure Apo-AI in Fig. 3a. To further evaluate whether interactions between Apo-AI and C_{16}-GGGRGDS modify the secondary structure, we compared measured CD spectrum with those calculated by the addition of the spectra for the individual components. Fig. 4 is a representative comparison showing a large difference between the measured and calculated spectra for one of the mixtures studied (M_r = 4.5). In this case, the calculated spectra corresponds to the one-to-one addition of the CD spectrum measured for 10.7 μM Apo-AI to the CD measured for 48 μM C_{16}-GGGRGDS (M_r = 48/10.7 = 4.5). The calculated CD spectra for M_r = 4.5 (Fig. 4) presents a maxima at 193 nm and a smaller minimum at 225 nm. This spectra is similar to that reported by us for C_{16}-KTTKS[32] and 154 μM C_{16}-GGGRGDS.[19] Our interpretation for the features in the calculated CD spectra for M_r = 4.5 (Fig. 4) is that they result from red-shifted β-sheet peaks associated with the lipopeptide fibrils,[33] the expected maximum for this structure being around 195–200 nm and the minimum being near 216 nm. In contrast, the CD spectra measured for M_r = 4.5 (Fig. 3–4) is dominated by an α-helical structure. Fig. 3 and Fig. 4 together indicate that there are interactions between Apo-AI and C_{16}-GGGRGDS which modify the secondary structure of each component, specifically there appears to be a decrease in α-helix content of Apo-AI and a reduction of β-sheet content of C_{16}-GGGRGDS.

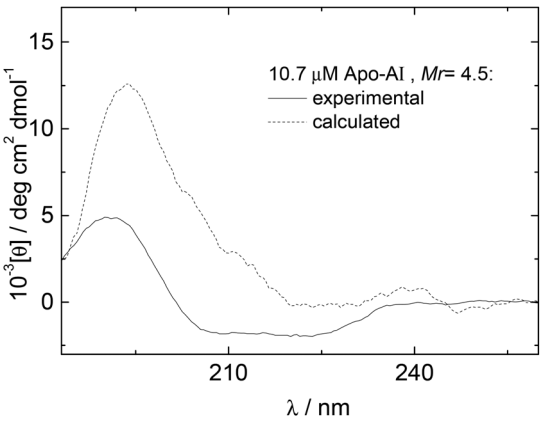

Fig. 4 (- - -) Experimental and (———) calculated CD data for M_r = 4.5.

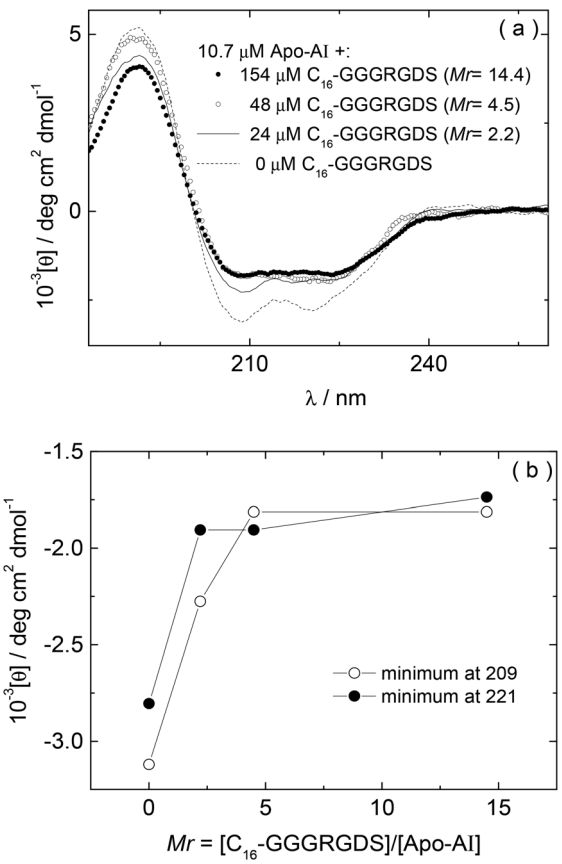

Fig. 3 (a) CD for Apo-AI/C_{16}-GGGRGDS mixtures measured as a function of M_r, (b) Dependence on M_r of the CD minima at 209 nm and 221 nm measured in (a).

According to the results from CD, the α-helical content of Apo-AI progressively reduces upon addition of C_{16}-GGGRGDS. In this way, the effect of lipopeptide titration into the Apo-AI solution is opposite to the interaction of Apo-AI with various lipids, in which case binding between the apolipoprotein and lipids leads to enhanced α-helix content.[9–11] However, the results from CD are in good agreement with ITC (Fig. 2), because it is possible that Apo-AI forms entropically favoured structures (such as aggregates) that might lead to the endothermic reaction measured by ITC experiments.

Cryo-TEM was used to image self-assembled structures in mixtures of Apo-AI and C_{16}-GGGRGDS above the saturation condition (M_r > 1). Fig. 5 shows cryo-TEM images measured for samples with 10.4 μM of Apo-AI and M_r = 2.2, 4.4 and 14.4. For the sample with M_r = 2.2, thin fibrils can be seen (Fig. 5a) with a diameter of approximately 10 nm. The fibrils are highly extended, with lengths up to tens of microns. Upon increasing the content of C_{16}-GGGRGDS in the solutions, the fibrils become more twisted as evident in Fig. 5b for M_r = 4.4. Of particular note, cryo-TEM shows a co-existence of fibrils and spheroidal aggregates for M_r = 2.2–14.4 (Fig. 5). The average

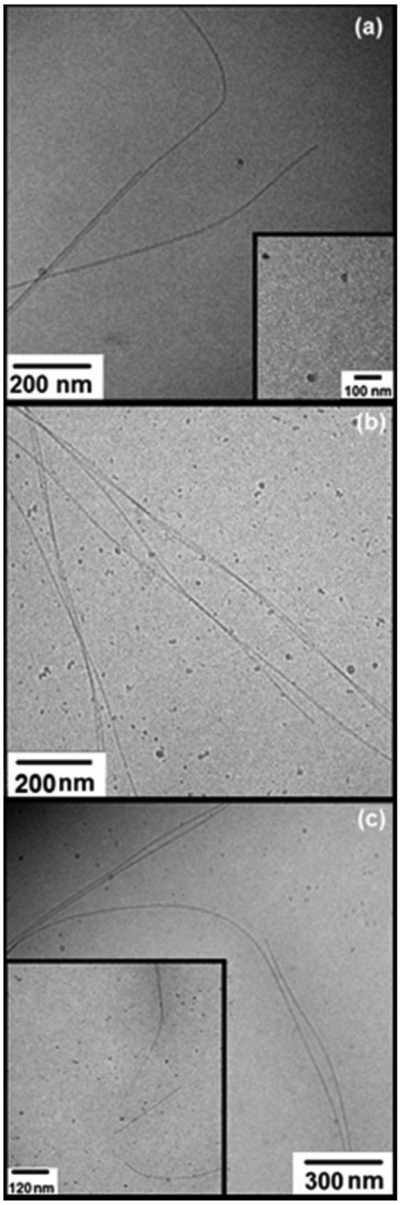

Fig. 5 Cryo-TEM images measured for samples with 10.4 μM of Apo-AI and M_r = (a) 2.2, (b) 4.4 and (c) 14.4. The insets in (a) and (c) show details of the aggregates observed for M_r = 2.2 and 14.4 respectively.

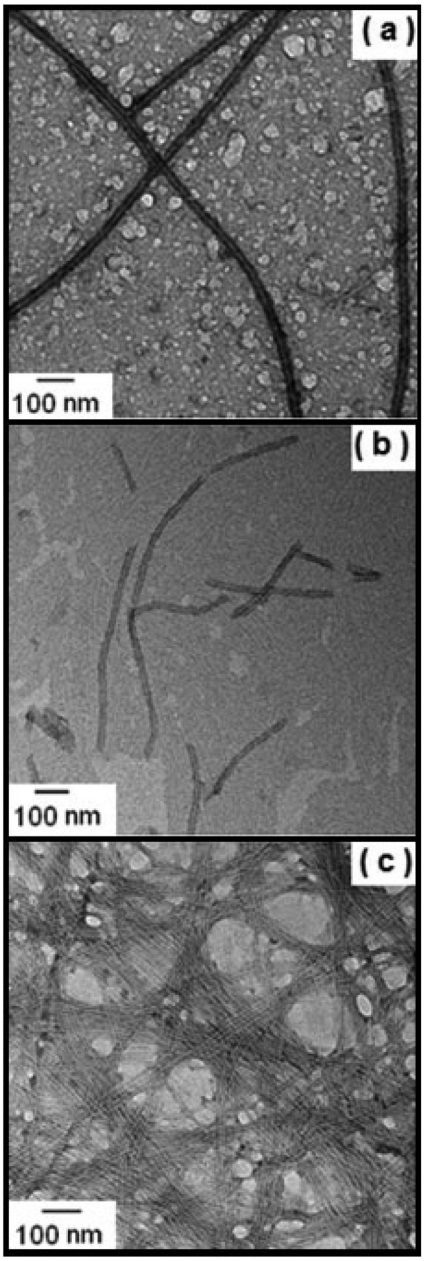

Fig. 6 TEM images measured for (a) 24, (b) 47 and (c) 154 μM C_{16}-GGGRGDS. (a), (b) and (c) are the control peptide solutions for the mixture samples with M_r = 2.2, 4.4 and 14.4 respectively.

size of these aggregates was (17.8 ± 4.2) nm, and did not show a particular dependence with M_r.

The aggregates shown in Fig. 5a–b have similar sizes to the 13 nm and ~(11.1–13) nm diameter nanodiscs formed through complexation of Apo-E with dipalmitoylphosphatidylcholine[34] and Human Apo-AI with dimyristoylphosphatidylcholine respectively.[7,34] Therefore, it is likely that the aggregates displayed in Fig. 5a–c arise from the complexation of the Apo-AI with C_{16}-GGGRGDS to form nanodiscs. This was further probed by SAXS (*vide infra*).

TEM experiments were performed for control solutions of C_{16}-GGGRGDS. The images displayed in Fig. 6 are for the lipopeptide solutions, with the same concentrations used to prepare solutions with M_r = 2.2, 4.4 and 14.4. Extended fibrils can be observed for all three concentrations, without amorphous aggregates in contrast to the mixtures with Apo-AI (Fig. 5). The formation of fibres is consistent with the low critical aggregation concentration for C_{16}-GGGRGDS, determined to be ~59 μM (in water).[19] Control experiments with Apo-AI only revealed no observable structures in TEM images at 10.7 μM concentration. It is evident that the irregular circular aggregates observed in Fig. 5 originate from the peptide/protein binding, since they are absent in Fig. 6.

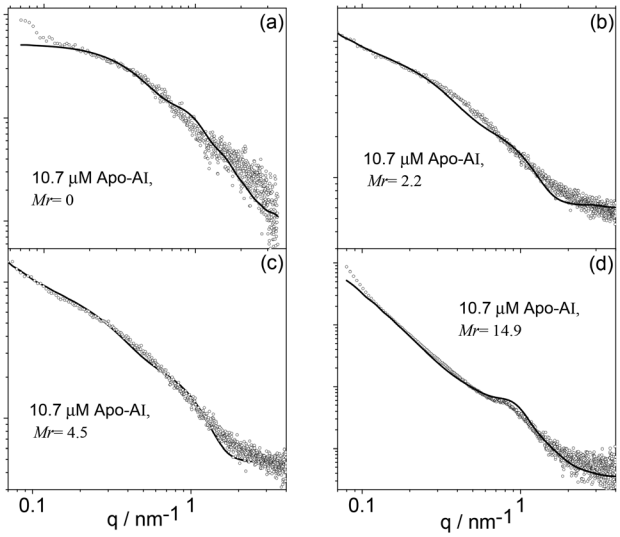

Fig. 7 SAXS data (symbols) along with calculated form factor profiles (full lines) according to the models described in the text. (a) M_r = 0, (b) M_r = 2.2, (c) M_r = 4.5 and (d) Mr = 14.9 (Table 1).

Consequently, the circular objects measured in Fig. 5 might be closely related to the nanodisc structures observed in previous lipid/Apo-AI binding studies.[7,8]

Electron microscopy imaging was complemented with SAXS experiments. The SAXS curves measured for 10 μM Apo-AI and Apo-AI/C_{16}-GGGRGDS mixtures above the saturation condition ($M_r > 1$) are displayed in Fig. 7. The resulting intensity profiles provide information on sample-averaged solution nanostructures, *via* analysis of the form factor. The form factor models are described in the Experimental section.

The form factor of Apo-AI (Fig. 6a) was computed from the published crystal structure as described in the SAXS Theory section and displayed in Fig. 1a. It agrees very well with the data. It has been shown that the Apo-AI is not monomeric for concentrations higher than 0.1 μM.[35] The crystallographic structure used to fit the experimental data corresponds to dimers of the C-terminal truncated apolipoprotein.[23] Indeed, attempts to model the observed SAXS data using published crystal structures for several monomeric forms of Apo-AI[6,36] were not successful. The presence of other oligomeric structures in the sample, as reported on the basis of analytical ultracentriguation experiments,[35] is highly probable, but a dimer model proved sufficient to fit the SAXS data.

Apparently, the incomplete loop structure of the Apo-AI dimer shown in Fig. 1a is, in the main, not able to wrap around the lipopeptide molecules to produce regular nanodiscs. However, cryo-TEM results show a few "nanodisc" structures in equilibrium with peptide nanofibres, suggesting that there is a dynamic competition between lipopeptide self-assembly and lipopeptide binding to Apo-AI.

Therefore, the SAXS data for M_r = 2.2–14.9 was modelled as a co-existence of flat cylinders with nanotape-like structures, which accounts for the mixture of extended fibrils and disk-like objects imaged/revealed by cryo-TEM (Fig. 5). The form factor for flat discs represents the Apo-AI/lipopetide aggregates, while the nanotape-like structure represents the C_{16}-GGGRGDS fibrils. The nanotape-like structure can be described using a lipid-like bilayer form factor in which the bilayer is represented by three Gaussian functions (one for the electron-depleted alkyl chain region and two for the headgroups at the surface of each bilayer) and has been previously used by us to describe C_{16}-GGGRGDS and related self-assembling peptide amphiphiles (PAs).[19] A structure factor for lamellar systems is used to account for the stacking of the bilayers within the PA tapes. The details of the form factors are given in the Experimental section. The SAXS data is displayed in Fig. 7b–d, together with the fitted curves using the corresponding form factors. The parameters obtained from the SAXS fitting are listed in Table 1.

The diameter of the flat discs used to fit data in Fig. 7b–d agrees with the size of the circular objects measured from the cryo-TEM images in Fig. 5. The estimated length of the extended C_{16}-GGGRGDS molecule is l_e = 42 Å, calculated by adding the length of a C_{16} chain (18 Å) to the total length of the peptide block (individual residue period of 3.4 Å).[37] The thickness of the bilayer $l_T \sim 2z_H + 2\sigma_H$ with Gaussian polydispersity Δ_{ZH} for z_H (Table 1), is shorter than two extended lipopeptides molecules $l_T < 2 \times l_e$ for M_r = 2.2–14.4, indicating that the C_{16} chain probably overlaps giving an interdigitated structure. It can also be noted that according to previous SAXS studies, pure C_{16}-GGGRGDS nanotapes are present in solution as a co-existence of two populations with d = 55 and 70 Å.[19] Binding of Apo-AI to C_{16}-GGGRGDS resulted in only one population of nanotapes with d = 65 Å (Table 1).

Table 1 Parameters extracted from the fitting of the SAXS data in Fig. 7b–d for samples containing 10 μM Apo-AI and C_{16}-GGGRGDS at different molar ratios M_r[a]

M_r	D [Å]	L [Å]	$2l_T$ [Å]	$10^4 \times \rho_H$ [rel. u.]	σ_H [Å]	$10^3 \times \rho_C$ [rel. u.]	σ_C [Å]	Co [a. u.]
2.2	106 ± 34	11.8	65 ± 5	1.9	2.5	−2.6	5	6
4.5	108 ± 34	11.8	65 ± 5	1.8	2.5	−2.7	5	4.5
14.9	108 ± 34	11.2	70 ± 5	0.09	5	−1.5	5	0.4

[a] N = 2, d = 65 Å and η = 0.4 in structure factor used only for M_r = 14.9.

Conclusions

The original aim of our work was to prepare lipopeptide/apolipoprotein nanodiscs, analogous to those reported for lipids but containing peptide-functionalised lipopeptide molecules wrapped with the Apo-AI. We have indeed observed a fraction of nanodiscs above the saturation binding condition, although these coexist with fibrillar structures from the lipopeptide self-assembly process.

We have shown that the lipopeptide C_{16}-GGGRGDS binds to Apo-AI with a saturation-binding type behaviour. The interaction is endothermic, which indicates that the binding process is driven by entropic processes which may correspond to changes in the conformation of the lipopeptide and/or apolipoprotein substrate. Circular dichroism spectroscopy provides a similar saturation binding concentration by monitoring the reduction in α-helical content of Apo-AI upon addition of C_{16}-GGGRGDS. There also seems to be a reduction in the β-sheet structure of C16-GGGRGDS. In other words, CD indicates conformational changes of both Apo-AI and lipopeptide. This points to the origin of the entropically driven process which leads to a loss of secondary structure as the two molecules interact.

Electron microscopy imaging reveals the presence of a mixture of fibrils and nanodiscs above the saturation binding condition. SAXS provided more insight into the nature of the self-assembly process and binding interaction. First, it confirms the findings from TEM of the presence of a mixture of fibrils and nanodiscs, also providing detailed (internal) structural parameters for these assemblies. Secondly, and most importantly, it shows that the Apo-AI itself is present in solution in the form of multimers, specifically dimers – although smaller amounts of other species may also be present. The fact that the Apo-AI was not present in monomeric form may be one reason why nanodiscs comprising Apo-AI wrapped around the lipopeptide were not able to assemble as the main morphology. A fibrillar structure was predominant, although some nanodiscs were seen reflecting the nature of the Apo-AI monomer/oligomer equilibrium as well as the lipopeptide self-assembly process and the possible interplay between these two equilibria in the mixed system.

This work forms part of a continuing effort to examine the bioactivity of biofunctional lipopeptides and further efforts to create lipopeptide nanodiscs are ongoing. Our work suggests that preparing Apo-AI in monomeric form may be critical to the synthesis of (entirely) nanodisc assemblies resulting from lipopeptide/apoliprotein complexation.

Acknowledgements

This work was supported by EPSRC grant EP/G026203/1. We would like to acknowledge A. Round and Barbara Calisto for support during beamtime sessions at the ESRF (Grenoble, France) beamline BM29 (Projects Number MX1511 and MX1620).

Notes and references

1 D. P. Rogers, L. M. Roberts, J. Lebowitz, J. A. Engler and C. G. Brouillette, *Biochemistry*, 1998, **37**, 945.
2 I. W. Hamley, *Chem. Rev.*, 2012, **112**, 5147.
3 K. Nagao, M. Hata, K. Tanaka, Y. Takechi, D. Nguyen, P. Dhanasekaran, *et al.*, *Biochim. Biophys. Acta, Bioenerg.*, 2014, **1841**, 80.
4 A. A. Ajees, G. M. Anantharamaiah, V. K. Mishra, M. M. Hussain and H. M. K. Murthy, *Proc. Natl. Acad. Sci. U. S. A.*, 2006, **103**, 2126.
5 W. S. Davidson, T. Hazlett, W. W. Mantulin and A. Jonas, *Proc. Natl. Acad. Sci. U. S. A.*, 1996, **93**, 13605.
6 D. W. Borhani, D. P. Roger, J. A. Engler and C. G. Brouillette, *Proc. Natl. Acad. Sci. U. S. A.*, 1997, **94**, 12291.
7 Y. Fang, O. Gursky and D. Atkinson, *Biochemistry*, 2003, **42**, 13260.
8 A. Nath, W. M. Atkins and S. G. Sligar, *Biochemistry*, 2007, **46**, 2059.
9 G. Franceschini, G. Vecchio, G. Gianfranceschi, D. Magani and C. R. Sirtori, *J. Biol. Chem.*, 1985, **260**, 6321.
10 H. Saito, P. Dhanasekaran, D. Nguyen, E. Deridder, P. Holvoet, S. Lund-Katz, *et al.*, *J. Biol. Chem.*, 2004, **279**, 20974.
11 S. E. Lux, R. I. Shrager, R. Hirz and A. M. Gotto, *J. Biol. Chem.*, 1972, **247**, 2598.
12 H. Saito, S. Lund-Katz and M. C. Phillips, *Progr. Lipid Res.*, 2004, **43**, 350.
13 A. Jonas, J. H. Wald, K. L. H. Toohill, E. S. Krul and K. E. Kezdy, *J. Biol. Chem.*, 1990, **265**, 22123.
14 J. P. Segrest, M. K. Jones, A. E. Klon, C. J. Sheldahl, M. Hellinger, H. De Loof, *et al.*, *J. Biol. Chem.*, 1999, **274**, 31755.
15 V. Castelletto, R. M. Gouveia, C. J. Connon, I. W. Hamley, J. Seitsonen, A. Nykanen, *et al.*, *Biomat. Sci.*, 2014, **2**, 362.
16 R. M. Gouveia, V. Castelletto, I. W. Hamley and C. J. Connon, *Adv. Healthcare Mater.*, 2014, Submitted.
17 M. J. Webber, J. Tongers, M.-A. Renault, J. G. Roncalli, D. W. Losordo and S. I. Stupp, *Acta Biomater.*, 2010, **6**, 3.
18 D. A. Harrington, E. Y. Cheng, M. O. Guler, L. K. Lee, J. L. Donovan, R. C. Claussen, *et al.*, *J. Biomed. Mat. Res., Part A*, 2006, **78A**, 157.
19 V. Castelletto, R. Gouveia, C. J. Connon and I. W. Hamley, *Faraday Discuss.*, 2013, **166**, 381.
20 J. D. Hartgerink, E. Beniash and S. I. Stupp, *Proc. Natl. Acad. Sci. U. S. A.*, 2002, **99**, 5133.
21 ATSAS. *Crysol - Version 2.8*, 1995–2011.
22 D. Svergun, C. Barberato and M. H. J. Koch, *J. Appl. Crystallogr.*, 1995, **28**, 768.
23 X. Mei and D. Atkinson, *J. Biol. Chem.*, 2011, **286**, 38570.
24 G. Pabst, M. Rappolt, H. Amenitsch and P. Laggner, *Phys. Rev. E: Stat. Phys., Plasmas, Fluids, Relat. Interdiscip. Top.*, 2000, **62**, 4000.
25 A. Caillé, *C. R. Acad. Sci. Paris*, 1972, **274**, 891.
26 R. Zhang, R. M. Suter and J. F. Nagle, *Phys. Rev. E: Stat. Phys., Plasmas, Fluids, Relat. Interdiscip. Top.*, 1994, **50**, 5047.

27 R. O'Brien and I. Haq. Applications of Biocalorimetry: Binding, Stability and Enzyme Kinetics, in *Biocalorimetry 2*, ed. J. E. Ladbury and M. Doyle, Wiley & Sons, London, 2004. pp. 3–34.
28 M. Kono, Y. Okumura, M. Tanaka, D. Nguyen, P. Dhanasekaran, S. Lund-Katz, *et al.*, *Biochemistry*, 2008, **47**, 11340.
29 C. Arnulphi, S. A. Sanchez, M. A. Tricerri, E. Gratton and A. Jonas, *Biophys. J.*, 2005, **89**, 285.
30 A. Derksen, D. Gantz and D. M. Small, *Biophys. J.*, 1996, **70**, 330.
31 L. Calabresi, G. Vecchio, R. Longhi, E. Gianazza, G. Palm, H. Wadensten, *et al.*, *J. Biol. Chem.*, 1994, **269**, 32168.
32 V. Castelletto, I. W. Hamley, J. Perez, L. Abezgauz and D. Danino, *Chem. Commun.*, 2010, **46**, 9185.
33 I. W. Hamley, D. R. Nutt, G. D. Brown, J. F. Miravet, B. Escuder and F. Rodriguez-Llansola, *J. Phys. Chem. B*, 2010, **114**, 940.
34 C. A. Peters-Libeu, Y. Newhouse, S. C. Hall, H. E. Witkowska and K. H. Weisgraber, *J. Lipid Res.*, 2007, **48**, 1035.
35 L. B. Vitello and A. M. Scanu, *J. Biol. Chem.*, 1976, **251**, 1131.
36 A. A. Ajees, G. M. Anantharamaiah, V. K. Mishra, M. M. Hussain and K. H. M. Murthy, *Proc. Natl. Acad. Sci. U. S. A.*, 2006, **103**, 2126.
37 T. E. Creighton, *Protein Folding*, W W. H. Freeman, New York, 1992.